

An unexplored regime of binary packing under extreme mixture conditions

Si Suo^{a,b,c}, Chongpu Zhai^{a,*}, Marc Kamlah^b, Yixiang Gan^{d,e,**}

^a State Key Laboratory for Strength and Vibration of Mechanical Structures, School of Aerospace, Xi'an Jiaotong University, Xi'an, China

^b Institute for Applied Materials, Karlsruhe Institute of Technology (KIT), Germany

^c Department of Engineering Mechanics, FLOW Centre, KTH, Stockholm SE-100 44, Sweden

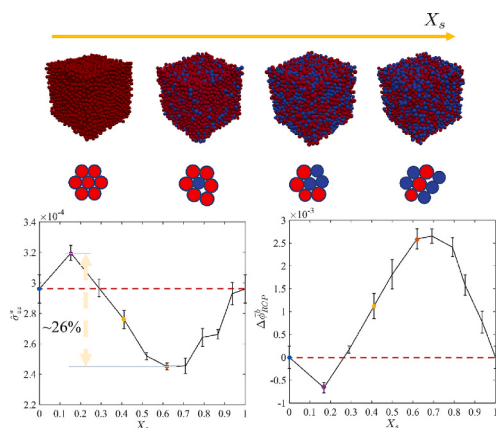
^d School of Civil Engineering, The University of Sydney, Sydney, NSW 2006, Australia

^e The University of Sydney Nano Institute (Sydney Nano), The University of Sydney, Sydney, NSW 2006, Australia

HIGHLIGHTS

- An unexplored regime of binary packing is shown to be looser than mono-sized one.
- Occurrence of this exceptional regime is statistically analysed and explained.
- Transition of binary RCP state is rationalized within modified hard-sphere scheme.

GRAPHICAL ABSTRACT



ARTICLE INFO

Keywords:

Granular packing
Binary packing
Discrete element method
Hard-sphere fluid theory

ABSTRACT

We present an unexplored regime, where the binary random close packing fraction ϕ_{RCP}^b is smaller than that of the mono-sized one ϕ_{RCP}^m . This is against previous observations and common perceptions that binary packing tends to be denser than mono-sized packing. We numerically confirm the critical condition for reaching this exceptional regime in the size ratio (R_r) and mole fraction (X_s) space, where R_r is close to 1, and the mole fraction of the smaller sphere X_s close to 0. Under the same loading condition, the stiffness of the packing at this exceptional regime is found to be significantly higher than that of the mono-sized packing. The formation and transition of this regime for varying R_r and X_s are theoretically modelled based on the hard-sphere fluid theory. This exceptional regime remains unreported in existing literature, yet significant for our fundamental understanding of binary packing systems.

* Corresponding author.

** Corresponding author at: School of Civil Engineering, The University of Sydney, Sydney, NSW 2006, Australia.

E-mail addresses: zhaichongpu@xjtu.edu.cn (C. Zhai), yixiang.gan@sydney.edu.au (Y. Gan).

1. Introduction

The random close packing (RCP) problem has attracted extensive attention, which is of great importance not only in our exploration into the fundamental physics of glasses, liquids, and colloidal systems [1], but also in facilitating the optimisation of conveying, handling, and processing different types of granular materials [2]. The RCP problem can be dated back to Bernal and Mason's experimental study on packings with identical spheres, in which the random close packing fraction for mono-sized packing, ϕ_{RCP}^m , was measured to be around 0.64 with an average coordination number, Z_c^m , of about 6 [3]. Following experimental and numerical studies [4–8] reported that ϕ_{RCP}^m generally ranges from 0.61 to 0.69. Despite great progress in both experimental and numerical studies [9–14], we still lack a comprehensive understanding of RCP, especially for binary packings, in terms of the particle-scale driving mechanism, collective behaviour of jamming development [15–17], tuneable properties including stiffness, mechanical stability [6], anti-crystallization [18,19], thermal and electrical conduction [20,21].

Few analytical approaches have been reported enabling satisfactory interpretation for the definition, formation, and characterization of mono-sized RCP. These models [22–25] simplify the structure evolution of RCP by concentrating on the contacting neighbours of an individual particle, while ignoring influences of non-contacting surrounding particles. Very recently, Zaccone [26] proposed a simple route based on the nearest-neighbour statistics towards the analytical solution for ϕ_{RCP}^m , with the effective boundary condition of $Z_c^m = 12$, $\phi_{RCP}^m \approx 0.74$, i.e., the known closest packing. No extra fitting parameters are required in this scheme, and the predicted ϕ_{RCP}^m highly matches the measurements from existing experiments and simulations. Noticeably, one could relate RCP to another critical packing fraction, named jamming density, at which the packing develops a mechanically stable structure that can reversibly withstand external loading with particle contacts percolating across the whole system [27–29]. Indeed, for the simplest case of mono-sized frictionless spheres, the jamming density (≈ 0.64) is around ϕ_{RCP}^m [30]. However, some studies based on the finite-size analysis [31,32] suggest that RCP appears far from the jamming point if particles are relatively soft, i.e., RCP could be over-jammed.

Regarding binary granular packings, the mixture can usually fill more space than mono-sized packings, with the corresponding RCP factor $\phi_{RCP}^b > \phi_{RCP}^m$. Theoretical solutions for both mono-sized packings [33] and binary mixtures [34] were developed based on equilibrium statistical mechanics. Recent studies [10–12,19,35] focus on situations with moderate or extremely small size ratio (small radius on large one), i.e., $R_r \rightarrow 0$. A quantity of empirical packing models were proposed based on the assumption that fine particles can fill the void among large particles [36–38]. However, the other near-boundary region, i.e., $R_r \rightarrow 1$, has seldom been investigated. One could intuitively expect the asymptotic trend to the mono-sized packing.

In this work, we remedy the unexplored region using numerical and theoretical approaches. We first provide numerical evidence for the existence of the so-called loose RCP state, which exhibits an “abnormal” valley in the regime transition from $\phi_{RCP}^b > \phi_{RCP}^m$ to $\phi_{RCP}^b < \phi_{RCP}^m$. Then, the occurrence of this exceptional regime is rationalized theoretically by the extension of Zaccone's scheme to the binary packing problem.

2. Simulations of binary packing

2.1. Numerical method

Numerical simulations are performed by the in-house code, KIT-DEM [21,39]. Each configuration is identified by the size ratio $R_r = d_s/d_l$ and mole fraction $X_s = N_s/(N_s + N_l)$. Here d_i and N_i are the particle diameter and number, and the subscripts s and l represent the small and large particles, respectively. At the initial state, 5000 frictionless non-cohesive

spherical particles are randomly packed within a periodic cubic domain [40]. The Hertzian contact model [41] is adopted, and the elasticity modulus is set large enough to guarantee the final particle-particle overlap is smaller than 0.1% particle radius.

All packings are uniaxially compressed using a quasi-static protocol [39] until reaching the RCP. Although the precise definition of RCP is still an open question and various criteria have been proposed [6,42,43], we adopt Bernal's criterion to define RCP, i.e., $Z_c = 6$ [3]. Then, the critical packing fraction ϕ_{RCP} is defined at $Z_c = 6$. For a given configuration, we carry out five realizations to examine the repeatability, and related quantities including packing fraction and stress are calculated as the mean values.

During the loading process, once crossing the critical point ($Z_c = 6$), as shown in Fig. 1(a), the packing starts jamming and its axial stress σ_{zz} significantly increases with strain ϵ . Under the same compression strain, packings with various mole fractions reach different stress levels, exhibiting varying packing stiffness. Here, we take characteristic stress σ_{zz}^* at $\epsilon = 5\%$ to characterize the post-jamming stiffness.

2.2. The unexpected valley of binary packing

Compared with mono-sized packing ($X_s = 0.00$), the mixture with a few small particles, such as $X_s = 0.17$ shown in Fig. 1(a), leads to a stiffer packing; however, further increasing X_s , the packing becomes relatively softer. As is detailed in Fig. 1(b), from the pure large-particle packing to the mixture, and further to the pure small-particle packing, σ_{zz}^* presents a peak-valley tendency. During compression, if a packing reaches RCP with a smaller normal strain, corresponding to a smaller critical packing fraction ϕ_{RCP} , its stress increases relatively faster, as is demonstrated by the stiffer strain-stress curve shown in Fig. 1(a). Therefore, over X_s , ϕ_{RCP} shows an inverse trend to σ_{zz}^* . Here, for the convenience of comparing ϕ_{RCP}^b and $\phi_{RCP}^m (=0.6494)$, we introduce a relative quantity $\Delta\bar{\phi}_{RCP}^b = \frac{\phi_{RCP}^b - \phi_{RCP}^m}{\phi_{RCP}^m}$.

The transition from the peak ($\Delta\bar{\phi}_{RCP}^b > 0$) to valley ($\Delta\bar{\phi}_{RCP}^b < 0$) with X_s ranging from 1 to 0 are clearly demonstrated in Fig. 1(c). Between these two regions, there exists a zero point $X_s^0(R_r)$ at which $\Delta\bar{\phi}_{RCP}^b = 0$, and for $R_r = 0.85$, X_s^0 is around 0.27. Though the lowest $\Delta\bar{\phi}_{RCP}^b$ appearing at the exceptional valley is just slightly smaller than that at the peak, their corresponding stresses shown in Fig. 1(b) demonstrate a difference of about 26% and this value is expected to be larger with further compressing. This suggests that the mechanical properties of the packing can be largely tuned by adding a small amount of small particles into the mono-sized packing.

To understand how much the large and small particles contribute to the RCP separately, we do statistics on the coordinate number of large and small particles at $Z_c = 6$, as shown in Fig. 2. For a mono-sized packing, the coordinate number approximately follows a normal distribution. Particles most likely have around six contact pairs and form a tight structure. When the packing is mixed with a bit of small particles, most small particles are bucklers whose coordinate numbers are less than six, while the coordinate number distribution of large particles slightly shifts to the right. It suggests that the original packing structures, centred by large particles, are mostly maintained. However, some looser but stable packing clusters appear locally due to the added small particles and lead to a smaller ϕ_{RCP}^b , as shown in Fig. 2(b). Furthermore, we compute the local packing fraction ϕ_{local} of each particle using Voronoi tessellation. The resulting histograms for large and small particles at various X_s are presented in Fig. 2(e) and (f), respectively. In comparison to the mono-sized packing ($X_s = 1$ and 0), the local packing fraction of large particles slightly increases due to the presence of mingled small particles. However, for small particles, ϕ_{local} is significantly smaller than the global packing fraction, indicating a higher degree of non-uniformity within the packing. This observation confirms

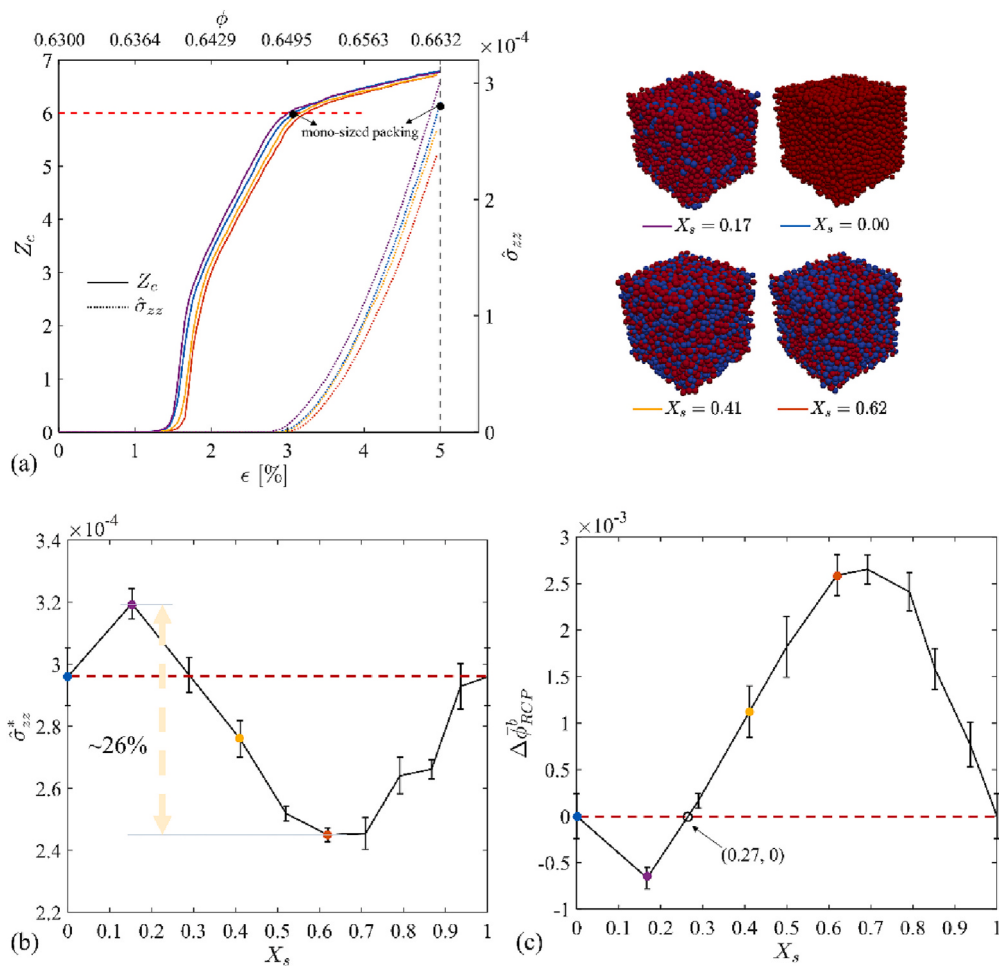


Fig. 1. (a) Non-dimensional axial stress $\hat{\sigma}_{zz}$ normalized by the elastic modulus of particles and average coordinate number Z_c vs. axial strain ϵ during loading for cases with a fixed $R_r = 0.85$ and various $X_s = 0.00, 0.17, 0.41$, and 0.62 . (b) Characteristic stress $\hat{\sigma}_{zz}^*$ and (c) relative random close packing $\Delta\phi_{RCP}^b$ vs. mole fraction X_s for $R_r = 0.85$. The cases in (a) are marked by solid spheres in (b) and (c) correspondingly.

the emergence of looser clusters, as shown in the insert of Fig. 2(b). With an increasing proportion of small particles, more contacts are built around small particles, effectively densifying the space together with large particles. With more small particles added, this constructed dense structure breaks down and the overall packing recovers to the original RCP structure but is dominated solely by small particles.

2.3. Pair correlation function

Moreover, we provide a close insight into this transition with the help of the pair correlation function $p(r)$ [44,45], which can measure the probability density of possible distances between centres of two particles (\vec{c}_i and \vec{c}_j) within a radial space $[r, r+dr]$. The function is defined as

$$p(r) = \frac{1}{\rho(N_s + N_l)} \sum_{\vec{c}_i} \sum_{\vec{c}_j} \delta \left[\left(|\vec{c}_i - \vec{c}_j| - r \right) \right] \bullet \left(r + dr - |\vec{c}_i - \vec{c}_j| \right) \frac{1}{4\pi r^2 dr}, \quad (1)$$

where ρ is the number density, i.e., $\rho = (N_s + N_l)/V$, and V is the domain volume. Peak values of $p(r)$ continuously occur but become hard to identify as r/d_l increases. Here, we focus on the range of $r/d_l < 3$. In Fig. 3(a), we present a schematic diagram of a three-layer structure surrounding a large particle, indicating that the majority of the packing is comprised of large particles. Small particles only appear in the third layer, implying that they have a relatively small contribution to the

packing. The distance between the central large particle and the third layer falls within the range of $[2.56d_l, 2.65d_l]$. Fig. 3 (b) ~ (f) demonstrate a transition from the loose to normal RCP state. From the variation of $p(r)$ with X_s , the third peak moves leftwards from $2.65d_l$, where large particles dominate the third layer, to smaller than $2.56d_l$, suggesting small particles break through the third layer into the second. In other words, the RCP state turns to normal (with the third peak of $2.65d_l$ in $p(r)$) from the loose one (with the third peak of $2.56d_l$ in $p(r)$) as we increase the number of small spheres in the mixture. Additionally, the second peak becomes obscure and even vanishes after the RCP state transition, see Fig. 3 (d) and (e), indicating s-l pairs contribute more to the second and third peaks in $p(r)$ and even dominate the third layer. Therefore, the impact of small particles on the third layer can be regarded as a meso-scale indicator for the RCP state, and the critical position of the third peak on $p(r)$ defines the phase boundary.

3. Hard-sphere fluid theory for binary systems

3.1. Theoretical development

In order to gain more understanding of this regime transition, we further provide a theoretical prediction on the binary RCP. Here, the hard-sphere (HS) fluid theory is employed for estimating the partial radial distribution functions (RDF) in binary packing, allowing the statistical description of the local structure around a sphere. Specifically, three types of sphere-to-sphere interaction, including small-small, large-

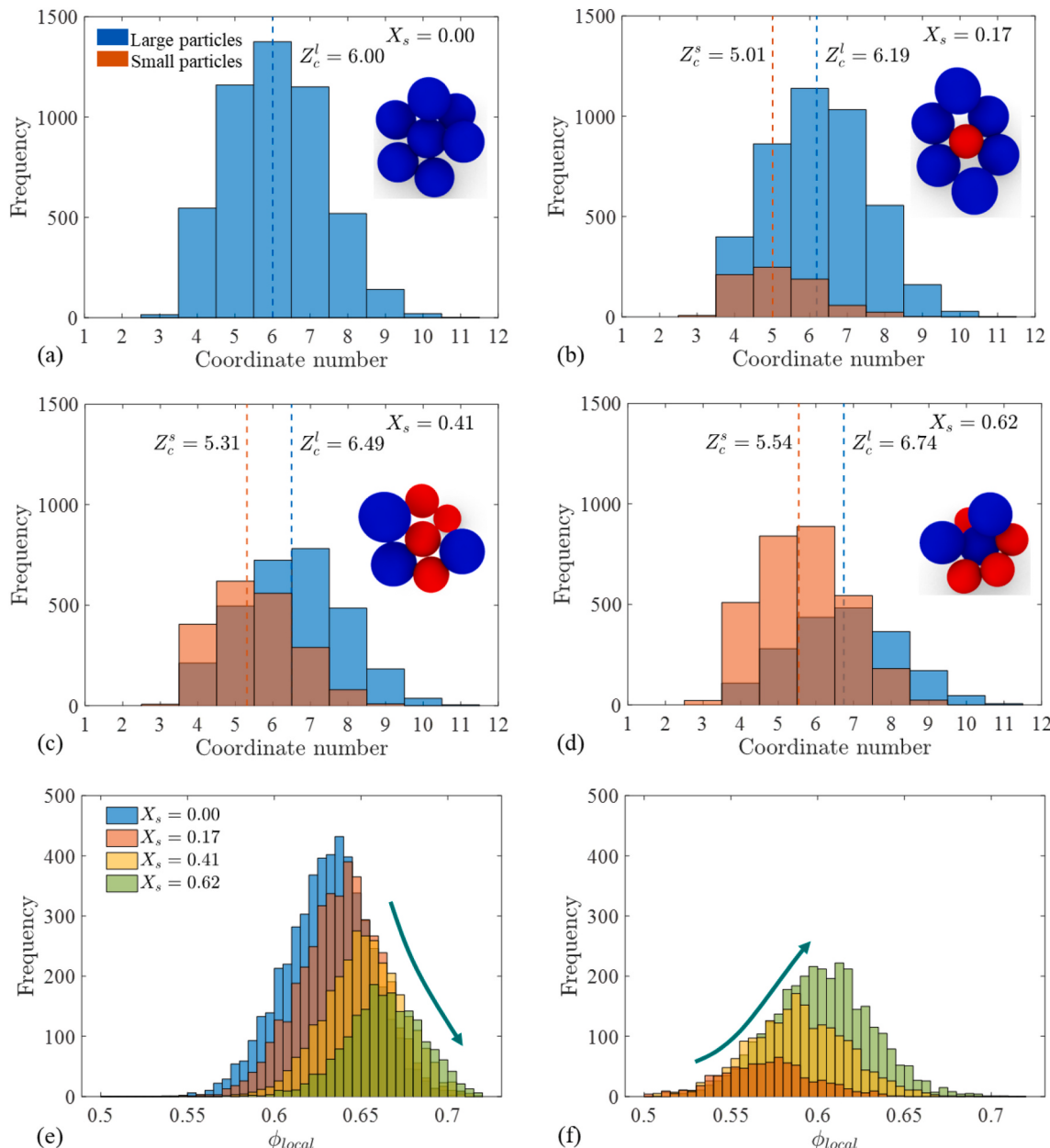


Fig. 2. Histograms of coordinate numbers for small and large particles at $X_s = 0.00$ (a), 0.17 (b), 0.41 (c), and 0.62 (d), which count all contacts around particles. The average coordinate number of small (Z_c^s) and large (Z_c^l) particles are highlighted. Histograms of local packing fraction ϕ_{local} are provided for large (e) and small (f) particles. The arrows indicate the direction of X_s growing.

large, and small-large pairs, with $g_{ss}(d)$, $g_{ll}(d)$ and $g_{sl}(d)$, respectively, indicate the probability density within a radial distance of d . Correspondingly, the contact value $Z_{c,ij}$ for the above three pair types (i,j for s or l) can be given by [26].

$$Z_{c,ij} = 4\pi\rho \int_0^{d_{ij}+\epsilon} g_{ij}^0 g_{ij}(d_{ij}) \delta(r - d_{ij}) r^2 dr, \quad (2)$$

where d_{ij} is the centre distance between two contacting spheres; g_{ij}^0 is a factor to be determined from the consistency conditions stated later. By weighting the contact value with mole fraction, the average coordination number Z_c^b of a binary packing is

$$Z_c^b(X_s, R_r) = X_s(Z_{c,ss} + Z_{c,sl}) + X_l(Z_{c,ll} + Z_{c,ls}), \quad (3)$$

where the mole fraction $X_l = N_l/(N_s + N_l)$. Naturally, the binary pack-

ing reduces to mono-sized packing, i.e., $Z_c^b(X_s, R_r)$ should be consistent with Z_c^m under the following situations, i.e., the so-called consistency conditions:

$$Z_c^b(0, R_r) = Z_c^m; Z_c^b(1, R_r) = Z_c^m; Z_c^b(X_s, 1) = Z_c^m. \quad (4)$$

Moreover, substituting Eq. (2) into Eq. (3), Z_c^b reads

$$Z_c^b = 4\pi\rho g^0 \left[X_s d_s^3 \tilde{g}_{ss}^0 g_{ss}(d_{ss}) + X_l d_l^3 \tilde{g}_{ll}^0 g_{ll}(d_{ll}) + d_{sl}^3 \tilde{g}_{sl}^0 g_{sl}(d_{sl}) \right], \quad (5)$$

where the factor g_{ij}^0 of Eq. (2) is expressed as $g_{ij}^0 = g^0 \tilde{g}_{ij}^0$. Here, g^0 is a normalization constant, and as followed by Zaccone's route [26], g^0 can be determined by introducing the conclusion of the mono-sized close packing ($Z_c^m = 12$, $\phi_{CP}^m \approx 0.74$); \tilde{g}_{ij}^0 is responsible for the consistency condition and therefore it is a function of X_s and normalized within

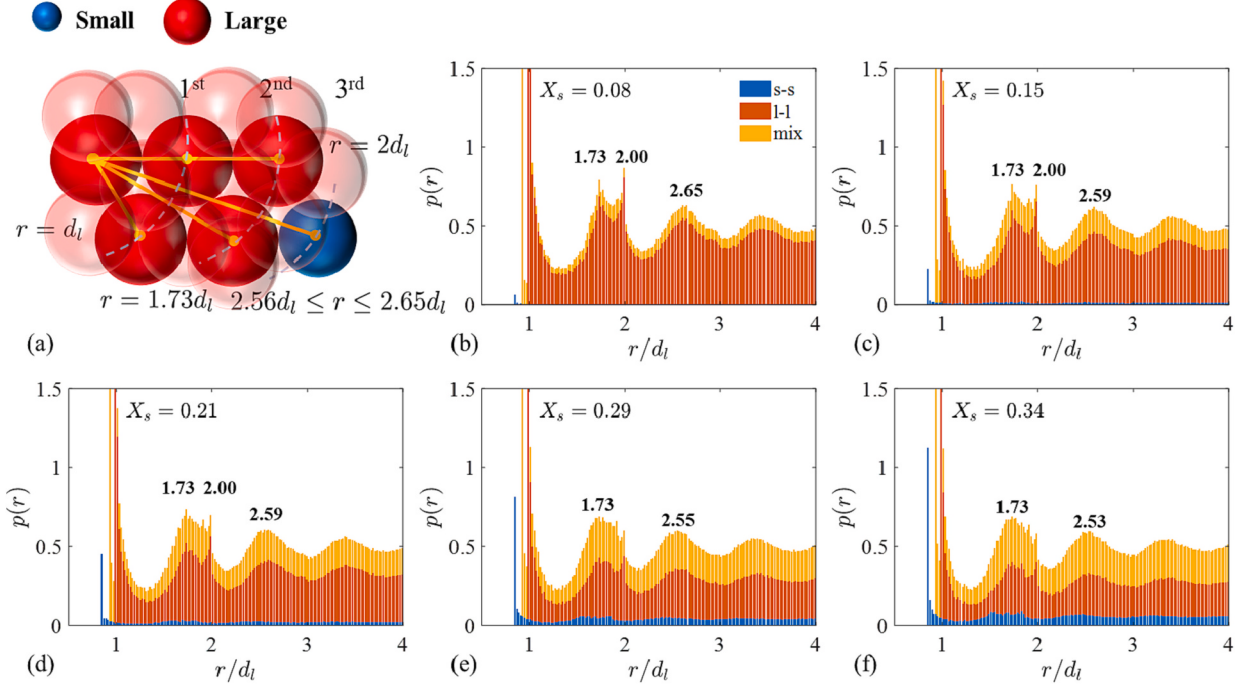


Fig. 3. The variation of pair correlation function $p(r)$ of $R_r = 0.85$ crossing the border of the loose RCP state with increasing X_s , i.e., from (b-d) locating within the valley region to (e-f) locating outside, and the corresponding positions on the R_r - X_s space can be referred to the symbol in Fig. 4(b). The values of r/d_l at the local peaks of $p(r)$ are indicated and can be referred to the particle-particle topology in (a).

[0, 1]. Specifically, corresponding to the consistency conditions, the constraints on \tilde{g}_{ij}^0 are given respectively by.

$$\tilde{g}_{ss}^0(0) = 0; \tilde{g}_{ss}^0(1) = 1; \quad (6)$$

$$\tilde{g}_{ll}^0(0) = 1; \tilde{g}_{ll}^0(1) = 0; \quad (7)$$

$$X_s \tilde{g}_{ss}^0(X_s) + (1 - X_s) \tilde{g}_{ll}^0(X_s) + \tilde{g}_{sl}^0(X_s) = 1 \quad (8)$$

Under the constraints of Eqs. (6)–(8), the possible format of \tilde{g}_{ij}^0 can be

$$\tilde{g}_{ss}^0(X_s) = X_s; \tilde{g}_{ll}^0(X_s) = 1 - X_s; \tilde{g}_{sl}^0(X_s) = 2X_s(1 - X_s). \quad (9)$$

Regarding $\tilde{g}_{ij}(d_{ij})$, the theory on additive HS mixtures, as an extension of the mono-component one, can provide a statistical solution, e.g., the BMCSL scheme [46] extended from the Carnahan-Starling equation [47]. It has been proved that the estimation on $g_{ij}(d_{ij})$ given by the original BMCSL expression is remarkably accurate for the moderate region of X_s and R_r , while for regions $X_s \rightarrow 0$ or $X_s \rightarrow 1$ of interest in this work, deviation occurs [48,49]. Thus, we employ a modified version which improved the BMCSL expression to fully satisfy the nine consistency conditions for binary mixtures by adding an additional term [49]. Moreover, in order to generate a quantitative description and better accommodate the theoretical framework, two adjustable indexes n_l and n_s are introduced on the additional term whilst all consistency conditions in [49] are respected. The final expressions, where $g_{ij}^{\text{BMCSL}}(d_{ij})$ is the contact value of the RDF from the BMCSL expression, explicitly read

$$g_{ll}(d_{ll}) = g_{ll}^{\text{BMCSL}}(d_{ll}) + \left(\frac{X_s}{4} \frac{\xi_1 \xi_2}{(1 - \xi_3)^2} \frac{d_{ll} - d_{ss}}{d_{sl}} d_{ll}^2 d_{ss} \right)^{n_l}, \quad (10)$$

$$g_{ss}(d_{ss}) = g_{ss}^{\text{BMCSL}}(d_{ss}) + \left(\frac{X_l}{4} \frac{\xi_1 \xi_2}{(1 - \xi_3)^2} \frac{d_{ll} - d_{ss}}{d_{sl}} d_{ss}^2 d_{ll} \right)^{n_s}, \quad (11)$$

$$g_{sl}(d_{sl}) = g_{sl}^{\text{BMCSL}}(d_{sl}) + \left(\frac{1}{4} \frac{\xi_1 \xi_2}{(1 - \xi_3)^2} \frac{d_{ll} - d_{ss}}{d_{sl}} \frac{d_{ll} d_{ss}^3}{d_{sl}} \right), \text{ and} \quad (12)$$

$$\xi_n = \frac{\pi}{6} \rho \sum_i X_i d_{ii}^n. \quad (13)$$

In the original BMCSL scheme [24], both n_l and n_s equal 1. Alternative modifications based on the BMCSL scheme can be referred to [50,51]. However, they can not output better predictions than Eqs. (10)–(13).

Substituting Eqs. (10)–(12) into Eq. (4) and setting $Z_c^b = 6$ establish an equation regarding ϕ_{RCP}^b , X_s and R_r , and thus we can solve ϕ_{RCP}^b on the R_r - X_s space. We first solve the distribution of ϕ_{RCP}^b based on the original expression in [49], i.e., $n_l = 1$ and $n_s = 1$, and compare our prediction against the reported data in [34]. As shown in Fig. 4(a), the prediction of our theory can capture the tendency of ϕ_{RCP}^b , i.e., an asymmetric distribution along X_s , which is also in agreement with direct observations from other experiments and simulations [12,19,52]. Furthermore, the solution quantitatively matches the reported data in the region $R_r \rightarrow 1$, though a noticeable deviation is observed in the moderate- R_r region ($R_r < 0.5$). The hard-sphere theory is developed based on the particle-scale configuration and is connected to the macroscopic equation-of-state (EOS). Different statistical models correspond to different EOSs. In the case of a binary mixture, its EOS varies across the range of R_r . While alternative models such as the Percus-Yevick theory [53] and Carnahan-Starling equation [47] may provide a good fit for the moderate- R_r region, they tend to lose accuracy as $R_r \rightarrow 1$. Therefore, we adhere to the current scheme as its solution is sufficiently accurate for the region of interest in our study.

3.2. Prediction of phase boundary

More important, the obtained theoretical prediction can reproduce the transition discovered in the above numerical experiments. In Fig. 4 (b), $\Delta\phi_{RCP}^b$ with respect to R_r and X_s extracted from all simulation cases

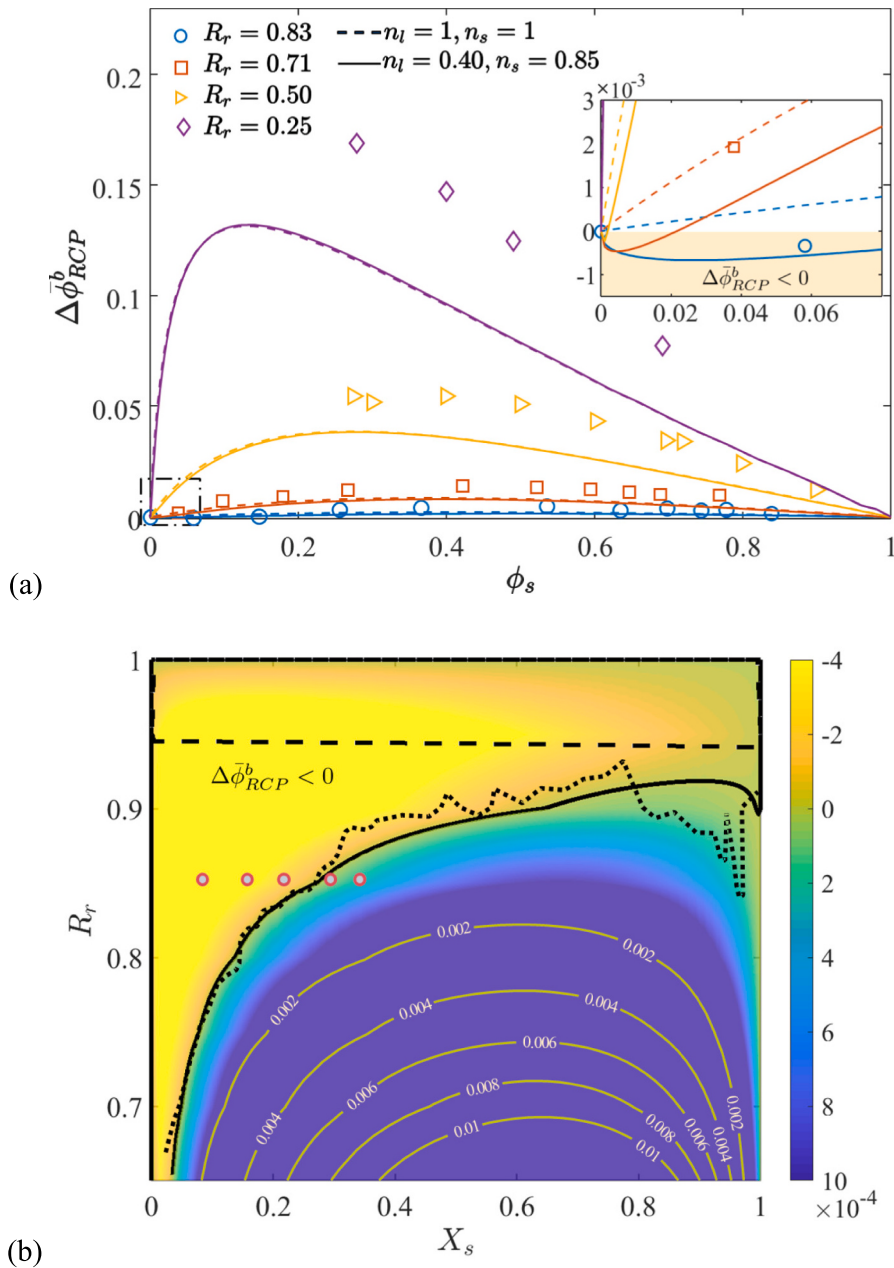


Fig. 4. (a) Relative packing fraction $\Delta\bar{\phi}_{RCP}^b$ vs. volume fraction of the small component, $\phi_s = X_s R_r^3 / (X_s R_r^3 + X_l)$. Open symbols are data reported in [34]; dash lines are theoretical predictions based on the Eqs. (10)–(12) with $n_l = 1$ and $n_s = 1$, while solid lines are the ones with $n_l = 0.40$ and $n_s = 0.85$. The subfigure is a zoom-in view of the near-boundary region ($X_s \rightarrow 0$). (b) The contour plot of the relative packing fraction $\Delta\bar{\phi}_{RCP}^b$ from simulations on the R_r - X_s space. The valley region appears in yellow. The dashed line represents the prediction by the original expression of $g_{ij}(d_{ij})$ in [49], with $n_l = 1$ and $n_s = 1$; the dotted line is extracted from simulation results; the solid line is predicted by Eqs. (10)–(12) with $n_l = 0.40$ and $n_s = 0.85$, selected for fitting the simulation data. The symbol \circ can be referred to Fig. 3 for further statistical analyses of the local packing structure of spheres. (For interpretation of the references to colour in this figure legend, the reader is referred to the web version of this article.)

are plotted. The valley of interest ($\Delta\bar{\phi}_{RCP}^b < 0$) as highlighted by the black line, which contains $X_s^0(R_r)$ extracted from numerical simulations and solved by the HS fluid theory. A good agreement to the simulation results (dotted line) can be obtained when $n_s = 0.40$ and $n_l = 0.85$ (solid line), as shown in Fig. 4(b). Besides, the original expression in [24] with $n_l = 1$ and $n_s = 1$ (dashed line) is also included for comparison. To be safe, we also test this modified version against the original version and the reported data. In Fig. 4(a), solutions based on the different groups of n_l and n_s are almost the same over the most range of ϕ_s , except in the range of $\phi_s \rightarrow 0$, see the insert. This suggests that modifying the additional terms in Eqs. (10) and (11) can only effectively influence the near-boundary range rather than the moderate R_r - X_s space. Moreover, the proposed expression with modified n_l and n_s is capable of predicting the loose RCP region, which is not only confirmed by our simulation results but also supported by the data reported in [34] on a qualitative basis, see the insert in the Fig. 4(a).

In summary, the asymmetry of packing fraction along mole

fraction was observed from our simulation and existing data in the literature. The original statistical model used in the hard-sphere fluid theory is capable of recovering the dependence of binary packings on R_r and X_s , and specifically such asymmetry is mainly from the cross-term $g_{sl}(d_{sl})$ in Eq. (13). Furthermore, we find that the looser binary packing should be owed to small particles distorting the typical compact structures, like trace impurities, as presented in our statistical analysis, which results in non-uniform structures. Our proposed model takes into account the contribution of small-small contacts to the non-uniformity, which is reflected by the indexes n_l and n_s introduced in $g_{ll}(d_{ll})$ and $g_{ss}(d_{ss})$.

4. Conclusions

In this work, we report a regime transition of binary packings from the loose RCP state, as compared to the mono-sized limit (i.e., $\phi_{RCP}^b < \phi_{RCP}^m$), to the normal one (i.e., $\phi_{RCP}^b > \phi_{RCP}^m$). The existence of the former regime is against our common understanding that a binary

packing should always be denser than a mono-sized one. This transition is confirmed through DEM simulations, and the exact phase boundary, $\phi_{RCP}^b = \phi_{RCP}^m$, of the loose RCP state can be established. The simulation also provides rich statistical information for this observed transition with an increasing fraction of smaller particles, during which small particles gradually dominate the third layer and are mixed into the second layer. Moreover, we have developed a theoretical model for binary packings by extending the recent model for mono-sized packing [26]. The proposed model has been validated against the data of binary packing reported in [34], and can predict the regime transition on the size ratio and mole fraction, R_r - X_s , space and quantitatively match the numerical observations. The implications of this unexpected regime are also demonstrated through the observed stiffness differences, which may result in different responses to external excitations.

In the future, this theoretical approach can be extended to polydisperse granular media [54,55]. Compared with the binary packing, it seems likely to realize much looser RCP packings by adjusting size distribution. Since mechanical and transport properties of granular materials are related to packing structures, this exceptional RCP state exhibits unique mechanical properties, such as more porosity and higher stiffness compared with mono-sized packing, potentially contributing to important engineering practices, such as lightweight concrete design [56], microstructure design of battery electrodes [57], and optimized granular beds for water retention [58,59], filtration [60,61], and thermal energy storage [62,63].

CRediT authorship contribution statement

Si Suo: Conceptualization, Methodology, Validation, Investigation, Data curation, Writing – original draft, Visualization. **Chongpu Zhai:** Conceptualization, Methodology, Validation, Investigation, Data curation, Writing – review & editing, Supervision. **Marc Kamlah:** Methodology, Resources, Writing – review & editing. **Yixiang Gan:** Conceptualization, Methodology, Resources, Writing – review & editing, Supervision.

Declaration of Competing Interest

The authors declare that they have no known competing financial interests or personal relationships that could have appeared to influence the work reported in this paper.

Data availability

Data will be made available on request.

Acknowledgments

This study is supported by No. LX6J018 and No. XZY012021003 from Xi'an Jiaotong University. The authors also gratefully acknowledge the financial support by the State Key Laboratory for Strength and Vibration of Mechanical Structures under SV2021-KF-27.

References

- [1] R.K. Annabattula, Y. Gan, M. Kamlah, Mechanics of binary and polydisperse spherical pebble assembly, *Fus. Eng. Des.* 87 (5) (2012) 853–858.
- [2] M. Oda, K.E. Iwashita, Mechanics of granular materials: An introduction, CRC press, 2020.
- [3] J.D. Bernal, J. Mason, Packing of spheres: co-ordination of randomly packed spheres, *Nature* 188 (4754) (1960) 910–911.
- [4] W.S. Jodrey, E.M. Tory, Computer simulation of close random packing of equal spheres, *Phys. Rev. A* 32 (4) (1985) 2347–2351.
- [5] J.G. Berryman, Random close packing of hard spheres and disks, *Phys. Rev. A* 27 (2) (1983) 1053–1061.
- [6] S. Torquato, T.M. Truskett, P.G. Debenedetti, Is random close packing of spheres well defined? *Phys. Rev. Lett.* 84 (10) (2000) 2064.
- [7] A.Z. Zinchenko, Algorithm for random close packing of spheres with periodic boundary conditions, *J. Comput. Phys.* 114 (2) (1994) 298–307.
- [8] G.D. Scott, D.M. Kilgour, The density of random close packing of spheres, *J. Phys. D. Appl. Phys.* 2 (6) (1969) 863–866.
- [9] K.W. Desmond, E.R. Weeks, Random close packing of disks and spheres in confined geometries, *Phys. Rev. E* 80 (5) (2009), 051305.
- [10] S. Pillitteri, et al., From jamming to fast compaction dynamics in granular binary mixtures, *Sci. Rep.* 9 (1) (2019) 7281.
- [11] I. Prasad, C. Santangelo, G. Grason, Subjamming transition in binary sphere mixtures, *Phys. Rev. E* 96 (5) (2017), 052905.
- [12] J.C. Petit, et al., Additional transition line in jammed asymmetric Bidisperse granular packings, *Phys. Rev. Lett.* 125 (21) (2020).
- [13] K.J. Dong, et al., Critical states and phase diagram in the packing of uniform spheres, *Europhys. Lett.* 86 (4) (2009) 46003.
- [14] X.Z. An, et al., On the relationships between structural properties and packing density of uniform spheres, *Powder Technol.* 388 (2021) 139–148.
- [15] R.P. Behringer, B. Chakraborty, The physics of jamming for granular materials: a review, *Prog. Phys.* 82 (1) (2018), 012601.
- [16] J.M. Ottino, D.V. Khakhar, Mixing and segregation of granular materials, *Annu. Rev. Fluid Mech.* 32 (1) (2000) 55–91.
- [17] X. An, C. Li, Q. Qian, Experimental study on the 3D vibrated packing densification of binary sphere mixtures, *Particuology* 27 (2016) 110–114.
- [18] N. Kumar, et al., Tuning the bulk properties of bidisperse granular mixtures by small amount of fines, *Powder Technol.* 293 (2016) 94–112.
- [19] S. Pillitteri, et al., How size ratio and segregation affect the packing of binary granular mixtures, *Soft Matter* 16 (39) (2020) 9094–9100.
- [20] C. Zhai, et al., Stress-dependent electrical transport and its universal scaling in granular materials, *Extrem. Mech. Lett.* 22 (2018) 83–88.
- [21] S. Suo, et al., Cyclic thermo-mechanical performance of granular beds: effect of elastoplasticity, *Powder Technol.* 394 (2021) 705–713.
- [22] C. Song, P. Wang, H.A. Makse, A phase diagram for jammed matter, *Nature* 453 (7195) (2008) 629–632.
- [23] R.D. Kamien, A.J. Liu, Why is random close packing reproducible? *Phys. Rev. Lett.* 99 (15) (2007), 155501.
- [24] J.A. Dodds, Simplest statistical geometric model of the simplest version of the multicomponent random packing problem, *Nature* 256 (5514) (1975) 187–189.
- [25] N. Ouchiyama, T. Tanaka, Porosity of a mass of solid particles having a range of sizes, *Ind. Eng. Chem. Fundam.* 20 (1) (1981) 66–71.
- [26] A. Zaccone, Explicit analytical solution for random close packing in \$d=2\$ and \$d=3\$, *Phys. Rev. Lett.* 128 (2) (2022), 028002.
- [27] S. Luding, Y. Jiang, M. Liu, Un-jamming due to energetic instability: statics to dynamics, *Granul. Matter* 23 (4) (2021).
- [28] S.N. Pathak, et al., Force percolation transition of jammed granular systems, *Phys. Rev. E* 96 (4) (2017), 042901.
- [29] T.S. Majmudar, et al., Jamming transition in granular systems, *Phys. Rev. Lett.* 98 (5) (2007), 058001.
- [30] S. Torquato, F.H. Stillinger, Jammed hard-particle packings: from Kepler to Bernal and beyond, *Rev. Mod. Phys.* 82 (3) (2010) 2633–2672.
- [31] P. Morse, et al., Differences in plasticity between hard and soft spheres, *Phys. Rev. Res.* 2 (2) (2020), 023179.
- [32] C.P. Goodrich, A.J. Liu, S.R. Nagel, Finite-size scaling at the jamming transition, *Phys. Rev. Lett.* 109 (9) (2012).
- [33] G. Parisi, F. Zamponi, The ideal glass transition of hard spheres, *J. Chem. Phys.* 123 (14) (2005), 144501.
- [34] I. Bazzoli, et al., Theory of amorphous packings of binary mixtures of hard spheres, *Phys. Rev. Lett.* 102 (19) (2009), 195701.
- [35] I. Srivastava, et al., Jamming of bidisperse frictional spheres, *Phys. Rev. Res.* 3 (3) (2021).
- [36] C.C. Furnas, Flow of Gases through Beds of Broken Solids vol. 307, US Government Printing Office, 1929.
- [37] F. De Larrard, Concrete Mixture Proportioning: A Scientific Approach, CRC Press, 1999.
- [38] A.B. Yu, N. Standish, A study of the packing of particles with a mixture size distribution, *Powder Technol.* 76 (2) (1993) 113–124.
- [39] Y. Gan, M. Kamlah, Discrete element modelling of pebble beds: with application to uniaxial compression tests of ceramic breeder pebble beds, *J. Mech. Phys. Solid* 58 (2) (2010) 129–144.
- [40] Y. Gan, M. Kamlah, J. Reimann, Computer simulation of packing structure in pebble beds, *Fus. Eng. Des.* 85 (10–12) (2010) 1782–1787.
- [41] C. Thornton, Granular Dynamics, Contact Mechanics and Particle System Simulations, Springer, 2015.
- [42] Z.H. Stachurski, Definition and properties of ideal amorphous solids, *Phys. Rev. Lett.* 90 (15) (2003).
- [43] N. Xu, J. Blawzdziewicz, C.S. O'Hern, Random close packing revisited: ways to pack frictionless disks, *Phys. Rev. E* 71 (6) (2005), 061306.
- [44] P. Riscone, E.I. Corwin, G. Parisi, Long-range anomalous decay of the correlation in jammed packings, *Phys. Rev. Lett.* 127 (3) (2021).
- [45] D. Frenkel, B. Smit, Understanding molecular simulation: From algorithms to applications vol. 1, Elsevier, 2001.
- [46] G.A. Mansoori, et al., Equilibrium thermodynamic properties of the mixture of hard spheres, *J. Chem. Phys.* 54 (4) (1971) 1523–1525.
- [47] N.F. Carnahan, K.E. Starling, Equation of state for nonattracting rigid spheres, *J. Chem. Phys.* 51 (2) (1969) 635–636.
- [48] B.D.H.L. Yau, K.-Y. Chan, D. Henderson, Pair correlation functions for a hard sphere mixture in the colloidal limit, *Mol. Phys.* 91 (6) (1997) 1137–1142.
- [49] C. Barrio, J.R. Solana, Consistency conditions and equation of state for additive hard-sphere fluid mixtures, *J. Chem. Phys.* 113 (22) (2000) 10180–10185.

- [50] D. Henderson, K.-Y. Chan, Solute-solvent pair distribution functions in highly asymmetric additive hard sphere mixtures, *J. Chem. Phys.* 108 (23) (1998) 9946–9947.
- [51] D. Henderson, K.-Y. Chan, Equation of state and correlation function contact values of a hard sphere mixture, *Mol. Phys.* 98 (15) (2000) 1005–1010.
- [52] S. Yerazunis, S.W. Cornell, B. Wintner, Dense random packing of binary mixtures of spheres, *Nature* 207 (4999) (1965) 835–837.
- [53] M.S. Wertheim, Exact solution of the Percus-Yevick integral equation for hard spheres, *Phys. Rev. Lett.* 10 (8) (1963) 321–323.
- [54] L.Y. Yi, et al., Coordination number of the packing of ternary mixtures of spheres: DEM simulations versus measurements, *Ind. Eng. Chem. Res.* 50 (14) (2011) 8773–8785.
- [55] C. Anzivino, et al., Estimating random close packing in polydisperse and bidisperse hard spheres via an equilibrium model of crowding, *J. Chem. Phys.* 158 (4) (2023), 044901.
- [56] D. Sari, A.G. Pasamehmetoglu, The effects of gradation and admixture on the pumice lightweight aggregate concrete, *Cem. Concr. Res.* 35 (5) (2005) 936–942.
- [57] X. Lu, et al., 3D microstructure design of lithium-ion battery electrodes assisted by X-ray nano-computed tomography and modelling, *Nat. Commun.* 11 (1) (2020).
- [58] S. Assouline, D. Tessier, A. Bruand, A conceptual model of the soil water retention curve, *Water Resour. Res.* 34 (2) (1998) 223–231.
- [59] J. Lu, et al., Root-induced changes of soil hydraulic properties – a review, *J. Hydrol.* 589 (2020), 125203.
- [60] P.F. Luckham, M.A. Ukeje, Effect of particle size distribution on the rheology of dispersed systems, *J. Colloid Interface Sci.* 220 (2) (1999) 347–356.
- [61] Y. Yu, et al., Filtration performance of the granular bed filter used for industrial flue gas purification: a review of simulation and experiment, *Sep. Purif. Technol.* 251 (2020), 117318.
- [62] S.M. Hasnain, Review on sustainable thermal energy storage technologies, part I: heat storage materials and techniques, *Energy Convers. Manag.* 39 (11) (1998) 1127–1138.
- [63] A. Gautam, R.P. Saini, A review on technical, applications and economic aspect of packed bed solar thermal energy storage system, *J. Energy Storage* 27 (2020), 101046.